CHEMISTRY
A EUROPEAN JOURNAL

DOI: 10.1002/chem.200701424

VIP

# Nucleation Process in the Cavity of a 48-Tungstophosphate Wheel Resulting in a 16-Metal-Centre Iron Oxide Nanocluster

**Sib Sankar Mal,[a] Michael H. Dickman,[a] Ulrich Kortz,*[a] Ana Maria Todea,[b] Alice Merca,[b] Hartmut Bögge,[b] Thorsten Glaser,[b] Achim Müller,*[b] Saritha Nellutla,[c] Narpinder Kaur,[c] Johan van Tol,[c] Naresh S. Dalal,*[c] Bineta Keita,[d] and Louis Nadjo*[d]**

*Dedicated to Professor Jerry Atwood on the occasion of his 65th birthday*

**Abstract:** The 16-$Fe^{III}$-containing 48-tungsto-8-phosphate $[P_8W_{48}O_{184}Fe_{16}(OH)_{28}(H_2O)_4]^{20-}$ (**1**) has been synthesised and characterised by IR and ESR spectroscopy, TGA, elemental analyses, electrochemistry and susceptibility measurements. Single-crystal X-ray analyses were carried out on $Li_4K_{16}[P_8W_{48}O_{184}Fe_{16}(OH)_{28}(H_2O)_4]\cdot 66\,H_2O\cdot 2\,KCl$ (**LiK-1**, orthorhombic space group *Pnnm*, $a=36.3777(9)$ Å, $b=13.9708(3)$ Å, $c=26.9140(7)$ Å, and $Z=2$) and on the corresponding mixed sodium–potassium salt $Na_9K_{11}[P_8W_{48}O_{184}Fe_{16}(OH)_{28}(H_2O)_4]\cdot 100\,H_2O$ (**NaK-1**, monoclinic space group *C2/c*, $a=46.552(4)$ Å, $b=20.8239(18)$ Å, $c=27.826(2)$ Å, $\beta=97.141(2)°$ and $Z=4$). Polyanion **1** contains—in the form of a cyclic arrangement—the unprecedented $\{Fe_{16}(OH)_{28}(H_2O)_4\}^{20+}$ nanocluster, with 16 edge- and corner-sharing $FeO_6$ octahedra, grafted on the inner surface of the crown-shaped $[H_7P_8W_{48}O_{184}]^{33-}$ (**$P_8W_{48}$**) precursor. The synthesis of **1** was accomplished by reaction of different iron species containing $Fe^{II}$ (in presence of $O_2$) or $Fe^{III}$ ions with the **$P_8W_{48}$** anion in aqueous, acidic medium (pH ≈4), which can be regarded as an assembly process under confined geometries. One fascinating aspect is the possibility to model the uptake and release of iron in ferritin. The electrochemical study of **1**, which is stable from pH 1 through 7, offers an interesting example of a highly iron-rich cluster. The reduction wave associated with the $Fe^{III}$ centres could not be split in distinct steps independent of the potential scan rate from 2 to 1000 $mV\,s^{-1}$; this is in full agreement with the structure showing that all 16 iron centres are equivalent. Polyanion **1** proved to be efficient for the electrocatalytic reduction of $NO_x$, including nitrate. Magnetic and variable frequency EPR measurements on **1** suggest that the $Fe^{III}$ ions are strongly antiferromagnetically coupled and that the ground state is tentatively spin $S=2$.

**Keywords:** electrochemistry · iron · magnetic properties · polyoxometalates · self-assembly

[a] S. S. Mal, Dr. M. H. Dickman, Prof. Dr. U. Kortz
Jacobs University Bremen
School of Engineering and Science
P.O. Box 750 561, 28725 Bremen (Germany)
Fax: (+49) 421-200-3229
E-mail: u.kortz@jacobs-university.de

[b] A. M. Todea, Dr. A. Merca, Dr. H. Bögge, Prof. Dr. T. Glaser, Prof. Dr. A. Müller
Fakultät für Chemie der Universität, Postfach 100131
33501 Bielefeld (Germany)
Fax: (+49) 521-106-6003
E-mail: a.mueller@uni-bielefeld.de

[c] Dr. S. Nellutla, N. Kaur, Dr. J. van Tol, Prof. Dr. N. S. Dalal
Department of Chemistry and Biochemistry
Florida State University and
National High Magnetic Field Laboratory and
Centre for Interdisciplinary Magnetic Resonance
Tallahassee, FL 32306–4390 (USA)
Fax: (+1) 850-644-8281
E-mail: dalal@chem.fsu.edu

[d] Dr. B. Keita, Prof. Dr. L. Nadjo
Laboratoire de Chimie Physique, UMR 8000, CNRS
Equipe d'Electrochimie et Photoélectrochimie
Université Paris-Sud, Bâtiment 350
91405 Orsay Cedex (France)
Fax: (+33) 169-154-328
E-mail: nadjo@lcp.u-psud.fr

Supporting information for this article is available on the WWW under http://www.chemeurj.org/ or from the author. It contains detailed electrochemical characterisation of **1**, with Figure S1. Figures S2–S4 show cyclic voltammograms of **1** and **$P_8W_{48}$** in the presence of nitrate and NO, and Figure S5 shows the thermogram of **LiK-1** from room temperature to 900 °C.

## Introduction

Chemistry under confined geometries—and this in a general sense—has attractive aspects which may be related to special topics of surface,[1a] geo-[1b] and especially biosciences.[2,3] One may ask general questions, such as: what is it like for molecules/ions to "live" inside a nanosized molecular container (or generally under constrained/shielded environmental conditions) with respect to the interactions between them? In this context we can refer to two scenarios: 1) such interactions take place (nearly) independent of the cavity-interior shell functionalities (as in a nano-test-tube) or 2) they are influenced by the shell functionalities. Whereas in the first case the situation allows the spectroscopic identification/characterisation of the species under consideration more easily than under bulk conditions, in the second case one can study template-directed syntheses leading to unprecedented nanospecies. Such a process occurs in nature in different types of compartments.[3] In the case of biomineralisation we can refer to the imposition of (biological) directionality on the chemistry of growth processes (vectorial regulation).[3] In the present study we consider templated nucleation processes based on hydrate complexes of $Fe^{II}$ (in presence of $O_2$) and $Fe^{III}$ in the cavity of the cyclic 48-tungstophosphate $\mathbf{P_8W_{48}}$ leading to an unprecedented 16-metal-centre iron oxide formed by linking $FeO_6$ octahedra. This type of nucleation is based on a breaking of symmetry during the assembly process caused by the template effect of the cavity internal WO groups. The mentioned reaction of $Fe^{II}$ in the presence of dioxygen shows an important feature: it played a key role on the early earth leading to iron-banded ores and is—regarding the confinement conditions—the basis for the formation of the iron oxide core of the metal-storage protein ferritin.[4a] In context with the present vectorial growth process, we should refer also to the bacterial Mo storage proteins, in which different specific pockets of the protein cavity direct in unique nucleation processes the formation of different polyoxometalates (POMs).[4b] The type of procedure/nucleation process described in this paper, which has several important interdisciplinary aspects, could in principle be extended to POMs with much larger cavities, for example, wheel-shaped polyoxomolybdates of the type $Mo_{176}$.[4c]

## Results and Discussion

**Synthesis and structure**: Although the $\mathbf{P_8W_{48}}$ cluster has been known for more than 20 years,[5] only recently the first examples of metal-containing derivatives have been reported. Pope's group prepared the first lanthanide derivative, $\{Ln_4(H_2O)_{28}[K\subset P_8W_{48}O_{184}(H_4W_4O_{12})_2Ln_2(H_2O)_{10}]^{13-}\}_x$ (Ln = La, Ce, Pr, Nd),[6] and Kortz and co-workers isolated the first transition-metal derivative, the 20-copper(II)-containing $[Cu_{20}Cl(OH)_{24}(H_2O)_{12}(P_8W_{48}O_{184})]^{25-}$[7] (see also the report on the $Cu_{20}$-azide derivative $[P_8W_{48}O_{184}Cu_{20}(N_3)_6(OH)_{18}]^{24-}$[8]), while Müller et al. discovered $[K_8\subset\{P_8W_{48}O_{184}\}\{V^V_4V^{IV}_2O_{12}(H_2O)_2\}_2]^{24-}$, containing two cationic $V_6$-type mixed-valence clusters and formed by an unprecedented nucleation process.[9] Very recently Kortz et al. reported $\{K(H_2O)\}_3\{Ru(p\text{-cymene})(H_2O)\}_4P_8W_{49}O_{186}(H_2O)_2]^{27-}$, which represents the first organometallic derivative of $\mathbf{P_8W_{48}}$.[10] Here we report on the iron derivative $[P_8W_{48}O_{184}Fe_{16}(OH)_{28}(H_2O)_4]^{20-}$ (**1**), which was identified independently in Bremen[11] and Bielefeld.

Polyanion **1** was isolated as the mixed cation salts $Li_4K_{16}[P_8W_{48}O_{184}Fe_{16}(OH)_{28}(H_2O)_4]\cdot 66\,H_2O\cdot 2\,KCl$ (**LiK-1**) and $Na_9K_{11}[P_8W_{48}O_{184}Fe_{16}(OH)_{28}(H_2O)_4]\cdot 100\,H_2O$ (**NaK-1**), see Experimental Section. Polyanion **1** contains an unprecedented $\{Fe_{16}(OH)_{28}(H_2O)_4\}^{20+}$ cluster in the cavity of $\mathbf{P_8W_{48}}$ with 16 edge- and corner-sharing $FeO_6$ octahedra being grafted to the inner surface of the "host" (see Figures 1 and 2).

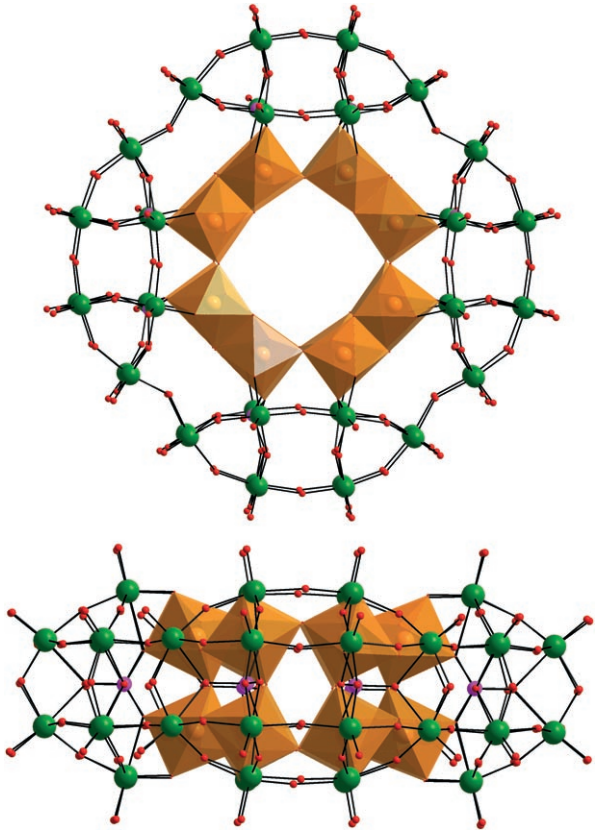

Figure 1. Front and side view of the structure of **1** emphasising the $FeO_6$ octahedra (brown) in polyhedral representation. Colour code: W (green), O (red), P (pink).

Polyanion **1** was generated by rather different synthetic procedures with respect to the type of iron precursors and the solvents (see Experimental Section). The Bremen group developed three slightly different synthesis procedures for **1** versus two of the Bielefeld group. For example, **1** can be prepared by reaction of a solution of $\mathbf{P_8W_{48}}$ with 1) $FeCl_3$ in 0.5 M $LiCH_3COO/CH_3COOH$ buffer, pH 4.0 and a few drops of 30% $H_2O_2$, 2) $Fe(ClO_4)_3$ in 0.5 M $LiCH_3COO/$

  

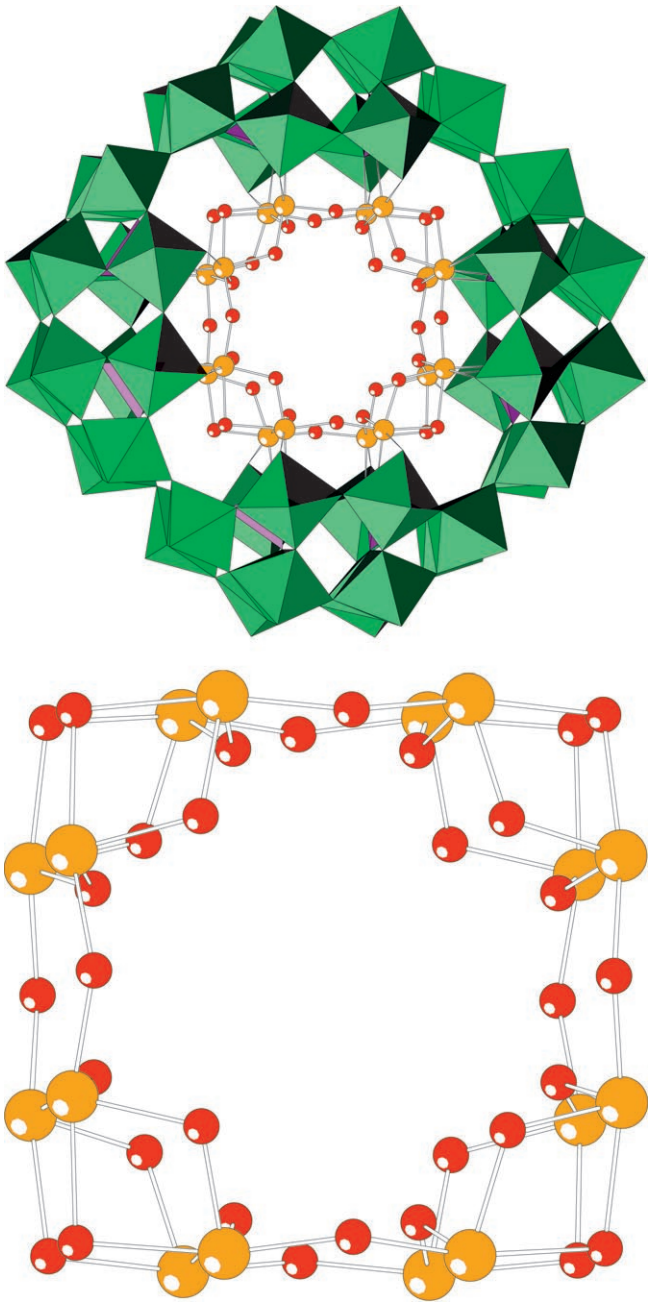

Figure 2. Top: Combined polyhedral/ball-and-stick representation of **1** emphasizing the connectivity of the central $\{Fe_{16}(OH)_{28}(H_2O)_4\}^{20+}$ cluster. Bottom: Ball-and-stick representation of the 16-iron-hydroxo cluster alone. Colour code: Fe (brown), O (red), $PO_4$ tetrahedra (pink), $WO_6$ octahedra (green).

$CH_3COOH$ buffer, pH 4.0, 3) $FeSO_4$ in 0.5 M $LiCH_3COO/CH_3COOH$ buffer, pH 4.0 and a few drops of 30% $H_2O_2$, 4) $[Fe_3O(CH_3COO)_6(H_2O)_3]Cl{\cdot}H_2O$ (**$Fe_3Ac_6$**) in 1 M $NaCH_3COO/CH_3COOH$ buffer, pH 4.2 and 5) $FeCl_2$ in 1 M $NaCH_3COO/CH_3COOH$ buffer, pH 4.2 in presence of $O_2$. Interestingly, the last reaction can be considered as a model for the formation of the iron(III) oxide nucleus of ferritin.

It became apparent that, as expected, the pH is a crucial parameter besides the acetate medium. On the other hand, it is possible to use a large variety of iron salts as starting materials, ranging from mononuclear iron(II) and iron(III) complexes (the former requires addition of an oxidant) to trinuclear iron(III) carboxylates. These observations support earlier knowledge that POM syntheses in general depend very much on the boundary conditions in the reaction vessel (e.g., pH and solvent).

Polyanion **1** exhibits a highly attractive symmetrical $D_{4h}$ structure (see Figures 1 and 2). The large cavity (roughly $9\times9\times7=567$ Å$^3$) of the "cyclic template/host" $\mathbf{P_8W_{48}}$ has been "decorated" with a cationic nanocluster built up by 16 $FeO_6$ octahedra, resulting in a smaller, central cavity (roughly $6\times6\times5=180$ Å$^3$). The related "$Fe_{16}$ ring" is composed of eight pairs of structurally equivalent, edge-shared $FeO_6$ octahedra that are connected to each other through corners. While most of the Fe-O-Fe bridges are monoprotonated, four are diprotonated (presence of $H_2O$ ligands). This can be confirmed by looking at the related bond valence sums (BVS) of these oxygen atoms.[12] For example, the protonated oxygens (with the corresponding BVS values) of the polyanion in the mixed lithium–potassium salt **LiK-1** are O14F (0.69), O23F (0.71), O13F (1.08), O24F (1.11), O14G (1.17), O23G (1.27), O1FE (1.31), O2FE (1.32), and O4FE (1.34), see Figure 3. The rather low, but "intermediate" (between mono- and diprotonation) BVS values of 0.69 and 0.71 for O14F and O23F, respectively, led us to believe that we are looking at a water and a hydroxo ligand disordered over these two sites. Hence, we should have a total of 28 hydroxo and 4 aqua ligands associated with **1**.

These results confirm that we have indeed grafted an unprecedented, cyclic $\{Fe_{16}(OH)_{28}(H_2O)_4\}^{20+}$ iron nanocluster with hydroxo and aqua ligands inside the cavity of $\mathbf{P_8W_{48}}$ (see Figures 1 and 2). Selected bond lengths and angles of the $\{Fe_{16}(OH)_{28}(H_2O)_4\}^{20+}$ unit are shown in Figure 3. The $FeO_6$ octahedra are only slightly distorted with Fe–O distances ranging from 1.985(12) to 2.153(12) Å.

It is of interest to compare the structure of **1** with $\mathbf{P_8W_{48}}$-type analogues containing other transition-metal centres. For example, we notice that the grafting mode of the 16 $Fe^{III}$ centres in **1** is different from that of the 20 $Cu^{II}$ centres in $[Cu_{20}Cl(OH)_{24}(H_2O)_{12}(P_8W_{48}O_{184})]^{25-}$.[7a] In **1** each of the 16 equivalent $Fe^{III}$ centres is bound to $\mathbf{P_8W_{48}}$ by a Fe–O(W) and a Fe–O(P) bond, resulting in a tight anchoring of the 16-iron–hydroxo core. In the $Cu_{20}$-POM, only eight of the 20 $Cu^{II}$ ions form two covalent Cu–O(W) bonds each to the $\mathbf{P_8W_{48}}$ host. Hence, the eight phosphate groups of $\mathbf{P_8W_{48}}$ are not involved in the binding to the cationic $\{Cu_{20}(OH)_{24}\}^{16+}$ cluster guest. In fact, **1** is structurally most closely related to Mialane's $Cu_{20}$-azide derivative $[P_8W_{48}O_{184}Cu_{20}(N_3)_6(OH)_{18}]^{24-}$.[8] In the latter, 16 of the 20 $Cu^{II}$ ions are bound to the inner rim of $\mathbf{P_8W_{48}}$ in exactly the same fashion as the $Fe^{III}$ centres in **1**. The sites of the remaining four unique, Jahn–Teller distorted $Cu^{II}$ ions in Mialane's POM remain empty in **1**. However, we believe that in principle these four sites could be filled in **1** as well; for example, by $Cu^{II}$ ions. In other words, there is a good chance that a mixed-metal (e.g., 16-iron-4-copper) derivative of **1** can be prepared.

  

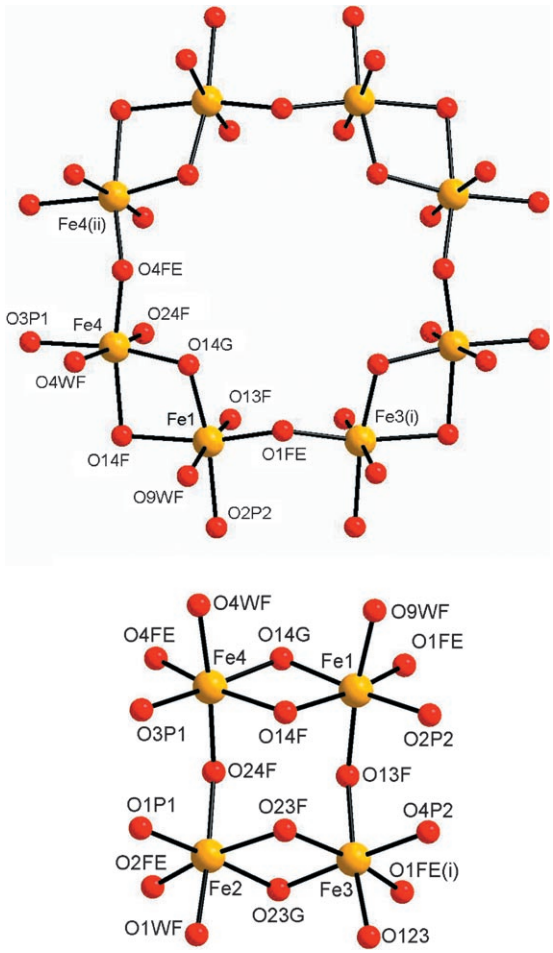


Figure 3. Top: Ball-and-stick view of a segment of **1**. Bottom: Side view including four independent $Fe^{III}$ centres. Oxygen atoms O9WF, O4WF, O1WF, and O123 bridge to atoms W9, W4, W1, and W12, respectively. Atoms O1P1, O3P1, O2P2, and O4P2 bridge to atoms P1 and P2. Selected distances (Å) and angles (°): Fe1–O1FE, 1.895(12); Fe1–O14G, 1.959(12); Fe1–O9WF, 1.964(12); Fe1–O13F, 1.972(12); Fe1–O2P2, 2.086(12); Fe1–O14F, 2.145(12); Fe2–O2FE, 1.905(6); Fe2–O23G, 1.942(12); Fe2–O1WF, 1.975(12); Fe2–O24F, 1.985(12); Fe2–O1P1, 2.067(11); Fe2–O23F, 2.140(13); Fe3–O1FE, 1.924(12); Fe3–O23G, 1.933(12); Fe3–O123, 1.964(12); Fe3–O13F, 1.975(12); Fe3–O4P2, 2.093(12); Fe3–O23F, 2.126(12); Fe4–O4FE, 1.903(6); Fe4–O14G, 1.950(12); Fe4–O24F, 1.951(12); Fe4–O4WF, 1.986(12); Fe4–O3P1, 2.103(11); Fe4–O14F, 2.153(12); Fe1-O14G-Fe4, 107.3(6); Fe1-O14F-Fe4, 94.2(5); Fe2-O23F-Fe3, 94.8(5); Fe2-O23G-Fe3, 108.3(6); Fe1-O13F-Fe3, 135.1(7); Fe2-O24F-Fe4, 136.1(6); Fe1-O1FE-Fe3(i), 139.6(7); Fe2-O2FE-Fe2(ii), 139.2(9); Fe4-O4FE-Fe4(ii), 137.5(9). All O-Fe-O angles are within 12.5(6)° of 90 or 180. Symmetry operations: (i), $-x$, $-1-y$, $z$; (ii), $x$, $y$, $-z$.

## Electrochemistry

*Stability studies*: UV/Vis spectroscopy and cyclic voltammetry (CV) were used to assess the stability of the title polyanion **1** by redissolving **LiK-1** in several aqueous media classically used as supporting electrolytes in electrochemical studies of POMs. Both techniques demonstrate that **1** is stable from pH 0.3 through 7. In this pH domain, its electronic spectra are characterised by an absorption peak located roughly at 350 nm and assigned to the $Fe^{III}$ centres in the structure and a second peak around 265 nm due to the tungstophosphate ligand framework $\mathbf{P_8W_{48}}$. The locations of these peaks depend on the pH. CV experiments, the duration of which can last up to 10 h, confirm also that **1** is stable in this pH domain.

*Voltammetric studies*: UV/Vis spectroscopy and CV studies indicate that **1** is stable from pH 0.3 through 7 and also its precursor $\mathbf{P_8W_{48}}$.[13] Figure 4 shows the CVs of **1** and $\mathbf{P_8W_{48}}$

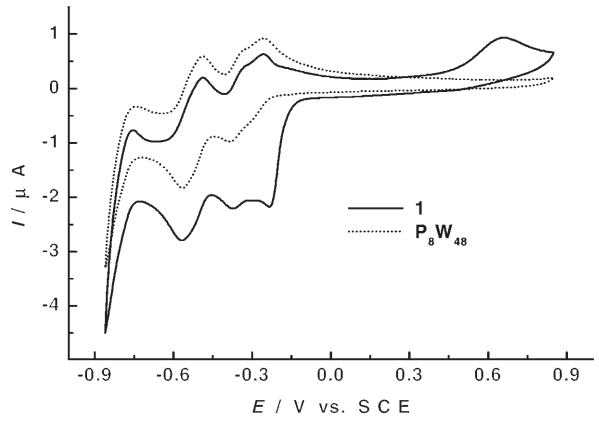


Figure 4. Superposition of the cyclic voltammograms of $4\times10^{-5}$ M **1** (full line curve) and $4\times10^{-5}$ M $\mathbf{P_8W_{48}}$ (dotted line curve) in pH 2 medium (0.5 M $Li_2SO_4/H^+$). The working electrode was glassy carbon and the reference electrode was SCE. The scan rate was 10 mV $s^{-1}$. For further details, see text.

in superposition. In the cathodic branch of the CV of **1**, is observed a reduction peak located at −0.220 V versus SCE, which does not exist in the pattern of the lacunary species $\mathbf{P_8W_{48}}$. This wave is assigned to the reduction of the $Fe^{III}$ centres. As a matter of fact, the $Fe^{III}$ centres are known to be more easily reduced than the $W^{VI}$ centres as seen in several iron-containing polytungstates.[14–16] For potential scan rates from 1000 down to 2 mV $s^{-1}$, no splitting of the single Fe-wave of **1** was observed. Controlled potential coulometry with the potential set at −0.230 V versus SCE indicates the consumption of 16 electrons per molecule. In addition, the characteristic blue colour of reduced W centres of most POMs was not observed during such reduction. These observations together confirm that this wave features the simultaneous one-electron reduction of the 16 $Fe^{III}$ centres in **1**. Reduction of all the 16 structurally equivalent Fe centres of **1** in a single step suggests that they are relatively independent, a feature that is reminiscent of the reduction process of certain polymers or dendrimers. Analogous examples can be found in POM electrochemistry.[16]

A detailed electrochemical study of **1** is provided in the Supporting Information (see Figures S1 and S2). These results underscore, at least, two important characteristics of **1**, which render this molecule a potential candidate for triggering electrocatalytic processes. Firstly, accumulation of several metallic centres associated with simultaneous electron

  

transfer and fairly fast kinetics is a necessary condition for reactions that require multiple electron transfers carried to completion and high efficiency. Secondly, the proximity of the $Fe^{III}$ and $W^{VI}$ waves of **1** can bring about beneficial effects.

To our knowledge, **1** constitutes the first example of multi-iron-containing POMs with such a small separation between the $Fe^{III}$ and the first W waves. The benefit of this property was demonstrated in the electrocatalytic reduction of nitrite by $Fe^{III}$-monosubstituted Wells–Dawson-type tungstates or molybdates.[17] Further examples were encountered in the electrocatalytic reduction of dioxygen and nitrogen oxides by $Cu^{2+}$-substituted tungstomolybdates.[18]

**Electrocatalytic behaviour of 1 towards $NO_x$**: The electrocatalytic reduction of nitrate remains a challenge in the $NO_x$ series because very few POMs are active in such electrocatalytic reduction.[19] The positive results observed with **1** are described in the Supporting Information. An exciting observation is described in the following.

*Reversible binding of NO to **1***: The interest in NO has grown considerably ever since its important role in biology, environment and industry was unveiled.

Very recently, we have demonstrated by CV that the following two POMs, $[Co(H_2O)_2\{(B\text{-}\beta\text{-}SiW_9O_{33}(OH))(\beta\text{-}SiW_8O_{29}(OH)_2)Co_3H_2O)\}_2]^{20-}$[19b] and $[\{Sn(CH_3)_2(H_2O)\}_{24}\{Sn(CH_3)_2\}_{12}(A\text{-}PW_9O_{34})_{12}]^{36-}$,[19c] interact reversibly with NO or related species. A similar, but much weaker interaction was detected for the plenary Wells–Dawson type tungstophosphate $[P_2W_{18}O_{62}]^{6-}$ and the plenary Keggin type tungstosilicate $[SiW_{12}O_{40}]^{4-}$. These observations suggest that the combination of large POM size and/or incorporation of $Co^{II}$ or diorganotin moieties favours interaction with NO, followed by efficient electrocatalytic reduction of NO.[19b,c]

With this prior knowledge in mind, we decided to study the interaction of **1** with NO, hoping for an associated catalytic activity of the polyanion towards the reduction of NO. For these experiments solutions of **1** at pH 1 were saturated in an alternating fashion with argon and NO, respectively. The main observations are illustrated in Figure 5; the potential domain is restricted to that of the composite wave recorded on a solution of **1** saturated with argon; it is composed of the $Fe^{III}$ reduction wave and the first $W^{VI}$ reduction wave of **1**. In the presence of NO an important catalytic current is observed that sets in at a more positive potential than that of the composite wave of **1**. In addition, the intensity of this catalytic wave increases strongly with time (Figure 5A). The cell was checked for leakage as explained in the Experimental Section.

An analogous behaviour is observed for $\mathbf{P_8W_{48}}$ in the presence of NO (Figure S3 in the Supporting Information), albeit with a roughly seven times weaker intensity than for **1** (Figure S4). However, this example permits to highlight details of the catalytic current. Figure 5B shows in superposition this catalytic process with its current scaled down to make its peak current match that observed in the presence

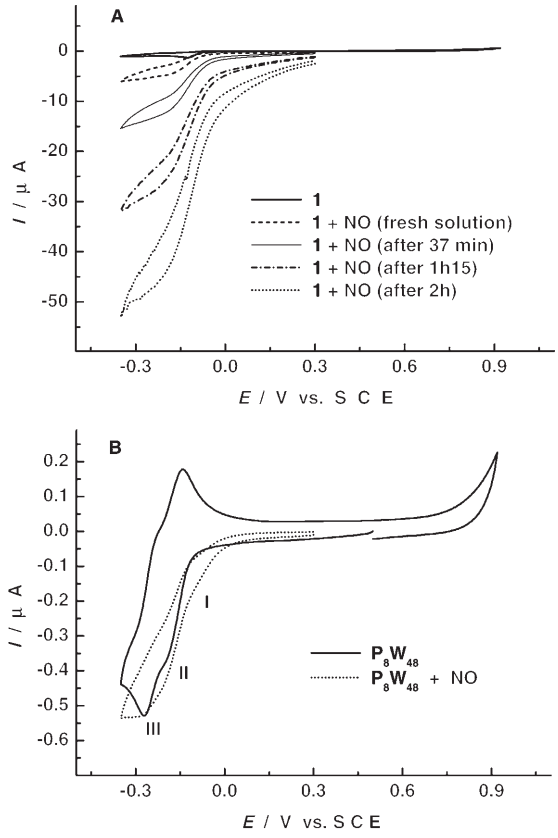


Figure 5. A) Cyclic voltammograms of $4\times10^{-5}$ M **1** at pH 1 in the presence of NO. The CVs are restricted to the potential domain of the composite wave recorded on a solution saturated with argon and comprising the $Fe^{III}$ reduction wave and the first $W^{VI}$-reduction wave of **1**, and at several time intervals after saturation with NO ([NO] = 1 to 2 mM). The working electrode was glassy carbon and the reference electrode was SCE. The scan rate was 2 mV $s^{-1}$. For further details, see text. B) Cyclic voltammograms of $4\times10^{-5}$ M $\mathbf{P_8W_{48}}$ at pH 1 saturated with argon or with NO, respectively. The current in the presence of NO was scaled down to make its peak current match that observed in the presence of argon. The working electrode was glassy carbon and the reference electrode was SCE. The scan rate was 2 mV $s^{-1}$. For further details, see text.

of argon. Three closely spaced waves can be distinguished, with the peak potential of the first one located roughly 0.1 V positive of the first wave of $\mathbf{P_8W_{48}}$. In short, this positive wave should be associated with a complex between NO and $\mathbf{P_8W_{48}}$. The same kind of complex is probably also present for **1**, but obscured by the $Fe^{III}$-wave, thus leaving only the overall positive shift of the catalytic wave. It must be noted that such shift is larger for **1** than for $\mathbf{P_8W_{48}}$. We found that NO can be eliminated by bubbling argon through the solutions and then voltammograms virtually identical to the original ones are restored for **1** and $\mathbf{P_8W_{48}}$.

Together, these observations indicate a reversible interaction between NO and **1** or $\mathbf{P_8W_{48}}$, followed by electrocatalytic reduction of NO.

**Magnetic susceptibility and EPR studies**: The molar magnetic susceptibility ($\chi_m$) and $\chi_m T$ of **LiK-1** as a function of temperature, $T$, are displayed in Figure 6. The observed

  

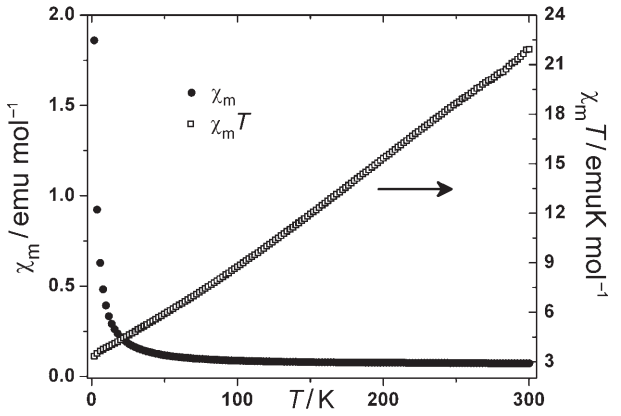


Figure 6. Magnetic susceptibility plotted as $\chi_m$ (●), $\chi_m T$ (□) versus $T$ for **LiK-1** powder.

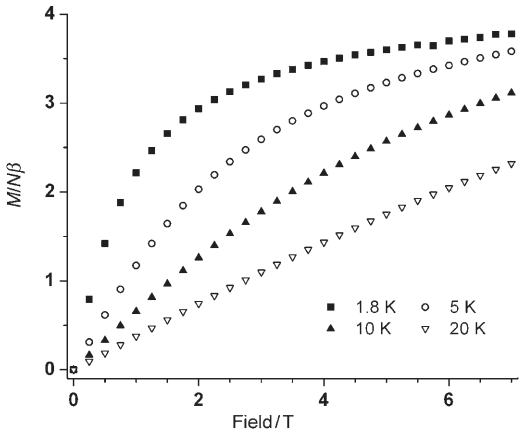


Figure 7. Magnetisation ($M/N\beta$) as a function of field for **LiK-1** powder plotted for various temperatures.

room-temperature $\chi_m T$ value of 21.9 emu K mol, when compared with that expected (70 emu K mol) for 16 non-interacting $Fe^{III}$ ($S=5/2$, $g=2$) ions, indicates that antiferromagnetic interactions play a dominant role in the title polyanion **1**. At 1.8 K, a $\chi_m T$ value of 3.3 emu K $mol^{-1}$ suggests that the ground state is $S_T=2$ (expected is 3 emu K $mol^{-1}$ with $g=2$).

The highly symmetrical $\{Fe_{16}(OH)_{28}(H_2O)_4\}^{20+}$ magnetic cluster incorporated in **1** is composed of 16 equivalent $Fe^{III}$ centres (see Figure 2). There are three types of Fe-O-Fe bridges (see Figure 3) that require three exchange coupling constants $J_1$ (e.g., Fe1-O1Fe-Fe3(i)), $J_2$ (e.g., Fe1-O14F/O14G-Fe4) and $J_3$ (e.g., Fe2-O24F-Fe4) and the interplay between them determines the ground state of **LiK-1**. The presence of 163112472594 spin states with a total spin $S_T$ ranging from 0 to 40 renders the detailed analysis of the magnetic susceptibility data of **LiK-1** complicated and is beyond the scope of the present study. However, a comparison of the Fe–O bond lengths and Fe-O-Fe bond angles of **1** with the literature values for $\mu_2$-hydroxo-bridged $Fe^{III}$ dimers and oligomers suggests that the magnitudes of $J_1$, $J_2$ and $J_3$ should be in the range of 20–25 $cm^{-1}$.[20,21] We hypothesise that the exchange couplings might be very similar in magnitude resulting in closely spaced spin levels and therefore the ground-state $S_T=2$ assignment can only be tentative. Although the absence of a plateau at around 3.3 emu K $mol^{-1}$ in the $\chi T$ profile supports our hypothesis, susceptibility measurements below 1.8 K are needed for confirmation.

Magnetisation ($M/N\beta$) versus field H for **LiK-1** at various temperatures is plotted in Figure 7. At 1.8 K, as the field increases from 0 to 7 T, $M/N\beta$ tends to reach 4, as expected for an $S=2$ spin system with $g=2$. The decrease in magnetisation as the temperature increases from 1.8 to 20 K could be due to the expected $H/T$ dependence of the magnetisation.[22]

In a further attempt to understand the magnetism of polyanion **1**, electron paramagnetic resonance (EPR) spectra were collected for various frequencies (9.65–319.2 GHz) and temperatures (5–300 K) for a powder sample of **LiK-1**. Only one broad peak ($\Delta H_{pp}=70\pm3$ mT) at $g=2.002\pm0.001$ is observed at room temperature for all experimental frequencies (see Figure 8). This is reminiscent of our earlier results on the hexa-$Fe^{II}$-substituted Keggin dimer $[Fe(OH)_3(A\text{-}\alpha\text{-}GeW_9O_{34}(OH)_3)_2]^{11-}$.[23] Figure 9 shows some typical X-band

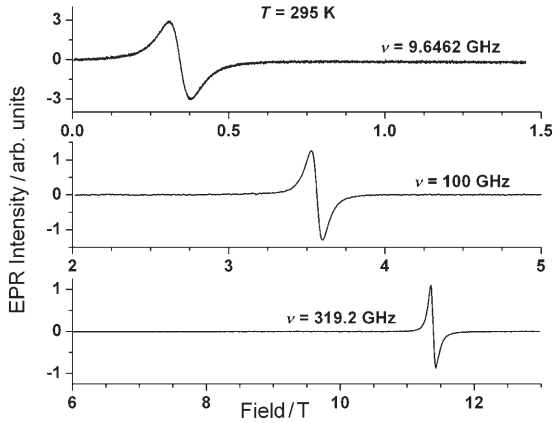


Figure 8. Room-temperature powder EPR spectra of **LiK-1** for 9.65, 100 and 319.2 GHz, respectively. Only one broad peak at $g=2.002$ is observed for all experimental frequencies.

(~9.65 GHz) and ~319 GHz spectra at a few temperatures. At least three features are evident: 1) a strong decrease in the signal intensity with decreasing temperatures, 2) signal broadening with decreasing temperatures and 3) absence of any additional splitting of the main peak. The intensity decrease is consistent with a similar trend in the magnetic susceptibility (Figure 6), and can thus be attributed to the population of states with smaller $S_T$ values at lower temperatures. On the other hand, signal broadening could be due to dipolar broadening and/or shorter relaxation times. The lack of any fine structure at all frequencies and temperatures studied renders it meaningless to derive any conclusions about the single-ion anisotropy of the overall $S_T$ value. The low temperature $g\sim4.3$ peak observed at X-band (indicated by * in Figure 9 top) is a $Fe^{III}$ impurity signal from the

  

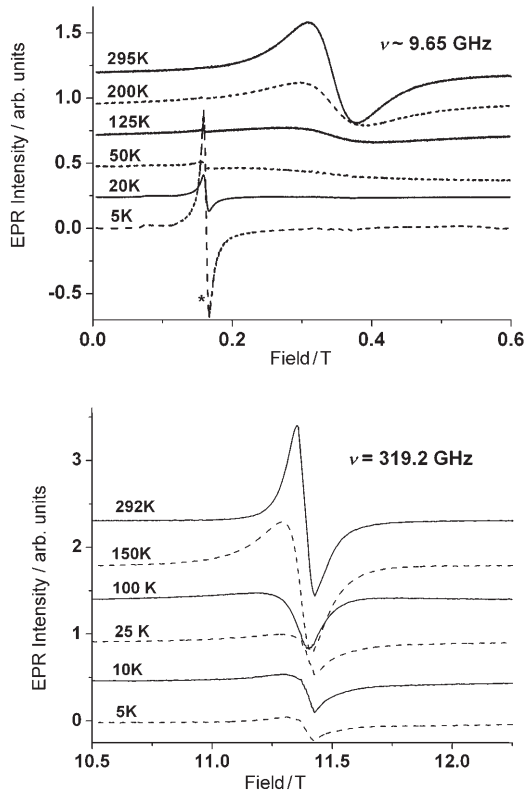


Figure 9. Temperature dependence of EPR spectra on **LiK-1** powder at ~9.65 GHz (top) and 319.2 GHz (bottom). The steady decrease of the signal intensity with decreasing temperature indicates the presence of excited states. The peak indicated by "*" at ~0.16 T in the top spectra is from a $Fe^{III}$ impurity in the sample.

sample. Finally, the small remnant signal observed at 319.2 GHz (see Figure 9 bottom) is attributed to a minor $g\sim 2$ impurity in the system and is not considered significant to the overall focus of the present study.

## Conclusion

We have prepared the 16-$Fe^{III}$ containing 48-tungsto-8-phosphate $[P_8W_{48}O_{184}Fe_{16}(OH)_{28}(H_2O)_4]^{20-}$ (**1**) as the mixed cation salts $Li_4K_{16}[P_8W_{48}O_{184}Fe_{16}(OH)_{28}(H_2O)_4]\cdot 66H_2O\cdot 2\,KCl$ (**LiK-1**) and $Na_9K_{11}[P_8W_{48}O_{184}Fe_{16}(OH)_{28}(H_2O)_4]\cdot 100H_2O$ (**NaK-1**). Polyanion **1** contains 16 edge- and corner-sharing $FeO_6$ octahedra in the form of a cyclic, unprecedented $\{Fe_{16}(OH)_{28}(H_2O)_4\}^{20+}$ iron–hydroxo–aqua nanocluster, grafted on the inner surface of the crown-shaped $[H_7P_8W_{48}O_{184}]^{33-}$ (**$P_8W_{48}$**) precursor. The synthesis of **1** was accomplished by reaction of hydrate complexes of $Fe^{II}$ (in presence of $O_2$), $Fe^{III}$ and $[Fe_3O(CH_3COO)_6(H_2O)_3]^+$ with **$P_8W_{48}$** in aqueous, acidic medium (pH ≈4).

Besides the unprecedented $\{Fe_{16}(OH)_{28}(H_2O)_4\}^{20+}$ iron–hydroxo–aqua nanocluster, the central (empty) cavity of the polyanion **1** has another highly interesting feature. Access of an oxidant/substrate to the "iron active site" is easily possible and therefore **1** is very attractive for catalytic applications. In fact, initial oxidation catalysis studies with air–oxygen as oxidant are highly promising.[11]

Furthermore, it is very likely that the cavity in **1** can be filled with additional metal centres, for example, those different from iron(III). We are currently engaged in the process of preparing mixed-metal derivatives of **1** (e.g., "$Fe_{16-x}M_xP_8W_{48}$") with one or more of the iron centres substituted by other transition-metal ions (e.g. $Mn^{II}$, $Co^{II}$, $Zn^{II}$). Such derivatives could lead to interesting magnetic as well as catalytic properties.[24]

The electrochemistry of **1** is characterised by a single 16-electron Fe-wave featuring the simultaneous reduction of all the $Fe^{III}$ centres, in full agreement with their structural equivalence. This wave could not be split into distinct steps whatever the potential scan rate from 2 to 1000 $mV\,s^{-1}$. Its potential location is very close to that of the first $W^{VI}$ wave of the lacunary precursor **$P_8W_{48}$**. Polyanion **1** shows efficient electrocatalytic properties regarding the reduction of $NO_x$, including nitrate. In addition, a remarkable reversible interaction between **1** and NO is observed. Such an interaction might justify investigating the biomimetic properties of this new POM.

The magnetic characterisation of **LiK-1** indicates that the ground state is made up of spin $S_T=2$, based on the data at 1.8 K. Even though we are unable to provide a quantitative estimate of the exchange interactions $J_1$, $J_2$ and $J_3$ we hypothesise that $J_1\approx J_2\approx J_3$ and the observed $S_T=2$ could be regarded as a tentative ground state of **1**. Additional measurements in the low-temperature range (<1.8 K) are needed to ascertain this prediction.

The study of a reaction of a solution of **$P_8W_{48}$** with metal cations offers the possibility to obtain basic information about principles of directed assembly processes under geometrically confined conditions. This can also lead, as in the present case, to cationic nanoclusters not obtainable under bulk conditions (see also reference [9]). One specific reaction described here refers to the "uptake of iron" under oxidative conditions and "release" under reducing conditions (the related simple reactions can be done under different reducing conditions) thereby mimicking the process occurring in the cavity of the protein ferritin. In this context one may also think about the option to study in a nanocavity the important reaction steps occurring during the reduction of $O_2$ with $Fe^{II}$, leading to $O_2^-$ and $OH^{\cdot}$[4a] even under simple "single-molecule type" conditions.

## Experimental Section

**Synthesis**: The precursor salt $K_{28}Li_5[H_7P_8W_{48}O_{184}]\cdot 92H_2O$ was synthesised according to the published procedure of Contant[25] and the purity was confirmed by infrared spectroscopy. All other reagents were used as purchased without further purification.

**$Li_4K_{16}[P_8W_{48}O_{184}Fe_{16}(OH)_{28}(H_2O)_4]\cdot 66H_2O\cdot 2\,KCl$ (LiK-1)**

*Method 1 (Bremen)*: A sample of $K_{28}Li_5[H_7P_8W_{48}O_{184}]\cdot 92H_2O$ (0.370 g, 0.025 mmol) was dissolved in $LiCH_3COO/CH_3COOH$ buffer (0.5 M, 20 mL) at pH 4.0. Then $FeCl_3\cdot 6H_2O$ (0.169 g, 0.625 mmol) was added and after complete dissolution, 30% $H_2O_2$ (10–20 drops) was added. Then

  

the solution was heated to 80 °C for 1 h and filtered while hot. After cooling to room temperature the filtrate was layered with around of KCl (1 M, 1 mL) solution. Slow evaporation in an open beaker at room temperature resulted in dark yellowish crystals after about one week. Evaporation was allowed to continue until the solution level had almost approached the solid product **LiK-1**, which was then collected by filtration, washed with cold water and air dried. Yield: 0.083 g (22 %). IR: $\tilde{\nu}$ = 1119 (sh), 1064 (s), 1019 (m; all $\nu_{as}$(P-O)), 951 (s), 927 (s, $\nu$(W=O)), 793 (s), 752 (s), 687 (s), 647 (sh) ($\nu_{as}$(W-O-W)), 559 (w), 526 (w), 473 $cm^{-1}$ (w); elemental analysis calcd (%) for **LiK-1**: Li 0.18, K 4.56, Fe 5.78, W 57.1, P 1.60, Cl 0.46; found: Li 0.24, K 4.73, Fe 5.35, W 58.1, P 1.60, Cl 0.28. The degree of hydration of **LiK-1** was determined by TGA (see Figure S5). Elemental analysis was performed by Mikroanalytisches Labor Egmont Pascher, An der Pulvermühle 3, 53424 Remagen, Germany.

*Method 2 (Bremen)*: A sample of $K_{28}Li_5[H_7P_8W_{48}O_{184}]\cdot 92H_2O$ (0.185 g, 0.0125 mmol) was dissolved in $LiCH_3COO/CH_3COOH$ buffer (0.5 M, 20 mL) at pH 4.0. Then $Fe(ClO_4)_3\cdot xH_2O$ (0.0974 g, 0.275 mmol) was added and the solution was heated to 80 °C for 1 h and filtered while hot. The following steps were identical to those of Method 1. The identity of **LiK-1** (isolated in very low yield, < 10 %) was established by XRD and IR.

*Method 3 (Bremen)*: A sample of $K_{28}Li_5[H_7P_8W_{48}O_{184}]\cdot 92H_2O$ (0.185 g, 0.0125 mmol) was dissolved in $LiCH_3COO/CH_3COOH$ buffer (0.5 M, 20 mL) at pH 4.0. Then $FeSO_4\cdot 7H_2O$ (0.0868 g, 0.313 mmol) was added and after complete dissolution, 30 % $H_2O_2$ (10–20 drops) was added. The colour of the solution changed to yellow. Then the solution was heated to 80 °C for 1 h and filtered while hot. The following steps were identical to those of Method 1. The identity of **LiK-1** (isolated in very low yield, < 10 %) was established by XRD and IR.

**$Na_9K_{11}[P_8W_{48}O_{184}Fe_{16}(OH)_{28}(H_2O)_4]\cdot 100H_2O$ (NaK-1)**

*Method 4 (Bielefeld)*: $K_{28}Li_5[H_7P_8W_{48}O_{184}]\cdot 92H_2O$ (0.67 g, 0.046 mmol) was dissolved in $NaCH_3COO/CH_3COOH$ buffer (1 M, 30 mL, pH 4.2). After $[Fe_3O(CH_3COO)_6(H_2O)_3]Cl\cdot H_2O$ {$Fe_3Ac_6$} (0.2 g, 0.31 mmol) was added, the solution was heated to 60 °C for 30 h and filtered after cooling it to room temperature. Slow evaporation in an open Erlenmeyer flask at room temperature resulted in the precipitation of dark yellowish crystals that were filtered off after 3 days; these crystals were washed with a small amount of cold water and dried in air. Yield: 0.09 g, 13 % (based on $P_8W_{48}$); elemental analysis calcd (%) for **NaK-1**: Na 1.30, K 2.71; found: Na 1.3, K 2.8. The identity of **NaK-1** was established by elemental analysis (in part done by Mikroanalytisches Labor Egmont Pascher, see above), IR spectroscopy and complete single-crystal X-ray structure analysis.

*Method 5 (Bielefeld)*: $K_{28}Li_5[H_7P_8W_{48}O_{184}]\cdot 92H_2O$ (0.35 g, 0.024 mmol) was dissolved in $NaCH_3COO/CH_3COOH$ buffer (1 M, 20 mL, pH 4.2). After $FeCl_2\cdot 4H_2O$ (0.1 g, 0.5 mmol) was added, the resulting solution was heated to 65 °C for 12 h and filtered after cooling to room temperature. Slow evaporation in an open Erlenmeyer flask at room temperature resulted in the precipitation of dark yellowish crystals that were filtered off after 7 days; these crystals were washed with a small amount of cold water and dried in air. Yield: 0.03 g, 8 %; elemental analysis calcd (%) for **NaK-1**: Na 1.30, K 2.71; found: Na 1.3, K 2.8. The identity of **NaK-1** was established by elemental analysis, XRD and IR spectroscopy.

**X-ray crystallography**

*Crystal data for $Li_4K_{16}[P_8W_{48}O_{184}Fe_{16}(OH)_{28}(H_2O)_4]\cdot 66H_2O\cdot 2$ KCl (**LiK-1**)*: A yellow crystal of **LiK-1** with dimensions $0.06\times 0.12\times 0.33$ $mm^3$ was mounted in oil on a Hampton cryoloop for indexing and intensity data collection at 173 K on a Bruker D8 APEX II CCD single-crystal diffractometer with $Mo_{K\alpha}$ radiation ($\lambda$ = 0.71073 Å). Of the 335706 reflections collected ($2\theta_{max}$ = 52.8°, 99.7 % complete), 14333 were unique ($R_{int}$ = 0.153) and 10468 reflections were considered observed [$I > 2\sigma(I)$]. The data were processed using SAINT (from Bruker AXS) and an absorption correction was performed using the SADABS program (G. M. Sheldrick, Bruker AXS). Direct methods were used to locate the tungsten atoms (SHELXS-97), and the remaining atoms were found from successive Fourier maps (SHELXL-97). No H or Li atoms were located. The final cycles of refinement on $F^2$ over all data included the atomic coordinates, anisotropic thermal parameters (W, Fe, P, Cl and non-disordered K atoms) and isotropic thermal parameters (O and disordered K atoms), converging to $R$ = 0.059 [$I > 2\sigma(I)$] and $R_w$ = 0.183 (all data). In the final difference map the deepest hole was −3.48 e $Å^{-3}$ (0.94 Å from W5) and the highest peak 4.20 e $Å^{-3}$ (0.73 Å from K4). The crystallographic data are provided in Table 1.

Table 1. Crystal data and structure refinement for $Li_4K_{16}[P_8W_{48}O_{184}Fe_{16}(OH)_{28}(H_2O)_4]\cdot 66H_2O\cdot 2$ KCl (**LiK-1**) and $Na_9K_{11}[P_8W_{48}O_{184}Fe_{16}(OH)_{28}(H_2O)_4]\cdot 100H_2O$ (**NaK-1**).

| | **LiK-1** | **NaK-1** |
|---|---|---|
| formula | $H_{164}Cl_2Fe_{16}K_{18}Li_8O_{282}P_8W_{48}$ | $H_{236}Fe_{16}K_{11}Na_9O_{316}P_8W_{48}$ |
| $M_r$ (g $mol^{-1}$) | 15473.7 | 15897.1 |
| crystal system | orthorhombic | monoclinic |
| space group (No.) | *Pnnm* (58) | *C2/c* (15) |
| *a* [Å] | 36.3777(9) | 46.5522(4) |
| *b* [Å] | 13.9708(3) | 20.8239(18) |
| *c* [Å] | 26.9140(7) | 27.8261(2) |
| *V* [$Å^3$] | 13678.4(6) | 26765.34(4) |
| *Z* | 2 | 4 |
| *T* [°C] | −73 | −90 |
| $\rho_{calcd}$ [Mg $m^{-3}$] | 3.76 | 3.945 |
| $\mu$ [$mm^{-1}$] | 21.37 | 21.74 |
| max/min transmission | 0.381/0.128 | 0.355/0.220 |
| data/parameters | 14333/492 | 29084/1584 |
| goodness-of-fit on $F^2$ | 1.02 | 1.08 |
| $R$ [$I > 2\sigma(I)$][a] | 0.059 | 0.109 |
| $R_w$ (all data)[b] | 0.183 | 0.303 |

[a] $R = \Sigma||F_o| - |F_c||/\Sigma|F_o|$. [b] $R_w = [\Sigma w(F_o^2 - F_c^2)^2/\Sigma w(F_o^2)^2]^{1/2}$.

*Crystal data for $Na_9K_{11}[P_8W_{48}O_{184}\ Fe_{16}(OH)_{28}(H_2O)_4]\cdot 100H_2O$ (**NaK-1**)*: A yellow crystal of **NaK-1** with dimensions $0.06\times 0.1\times 0.1$ $mm^3$ was removed from the mother liquor and immediately cooled to 183(2) K on a Bruker AXS SMART diffractometer (three-circle goniometer with 1 K CCD detector, $Mo_{K\alpha}$ radiation, graphite monochromator; hemisphere data collection in $\omega$ at 0.3° scan width in three runs with 606, 435 and 230 frames ($\varphi$ = 0, 88 and 180°) at a detector distance of 5 cm). A total of 78576 reflections (1.48 < $\Theta$ < 27.05°) were collected of which 29084 reflections were unique ($R_{int}$ = 0.1127). An empirical absorption correction using equivalent reflections was performed with the program SADABS 2.03. The structure was solved with the program SHELXS-97 and refined using SHELXL-97 to $R$ = 0.1088 for 14786 reflections with $I > 2\sigma(I)$, $R$ = 0.1935 for all reflections; max/min residual electron density 5.573 and −2.272 e $Å^{-3}$. (SHELXS/L, SADABS from G. M. Sheldrick, University of Göttingen 1997/2003; structure graphics with DIAMOND 2.1 from K.Brandenburg, Crystal Impact GbR, 2001.)

Further details of the crystal structure investigations may be obtained from the Fachinformationszentrum Karlsruhe, 76344 Eggenstein-Leopoldshafen, Germany (Fax: (+49) 7247-808-666; e-mail: crysdata@fiz-karlsruhe.de) on quoting the depository number CSD-418194 (**LiK-1**) and CSD-418527 (**NaK-1**).

**UV/Vis spectroscopy**: Pure water was used as solvent throughout, which was obtained by passing through a RiOs 8 unit followed by a Millipore-Q Academic purification set. All reagents were of high-purity grade and were used as purchased without further purification. The UV/Vis spectra were recorded on a Perkin–Elmer Lambda 19 spectrophotometer on $1.6\times 10^{-5}$ M solutions of **LiK-1**. Matched 1.000 cm optical path quartz cuvettes were used. The following media proved useful for the present study: 0.5 M $H_2SO_4$ pH 0.30; 1 M LiCl/HCl, pH 1 to 3; 1 M $CH_3CO_2Li/CH_3CO_2H$, pH 5 to 7.

**Electrochemical experiments**: The solutions were deaerated thoroughly for at least 30 min with pure argon and kept under a positive pressure of this gas during the experiments. NO was introduced in an oxygen-free electrochemical cell through a catheter connected to a sealed purging system previously filled with argon, which excluded oxygen and allowed

  

contaminants such as $NO_x$ to be scavenged in 9 M KOH. NO was bubbled through the electrolyte in the electrochemical cell for 30 min, resulting in a NO-saturated solution (1–2 mM). The electrochemical cell was checked for leaks in the following way: solutions saturated with NO were kept for several hours and used for electrocatalytic reduction of this substrate; after removing NO by bubbling pure argon, no electroactivity of NO or a related species could be detected in the potential range from +0.920 V to −0.730 V at pH 1.

The source, mounting and polishing of the glassy carbon (GC) electrodes have been described previously.[26] The glassy carbon samples had a diameter of 3 mm. The electrochemical set-up was an EG & G 273 A driven by a PC with the M270 software. Potentials are quoted against a saturated calomel electrode (SCE). The counter electrode was a platinum gauze of large surface area. All experiments were performed at room temperature.

**Magnetic measurements**: Magnetic susceptibility and magnetisation measurements were carried out on powder samples of **LiK-1** using a Quantum Design MPMS SQUID magnetometer in the temperature range of 1.8–300 K and field range of 0–7 T. The data were corrected for the sample holder, TIP of $Fe^{3+}$, $W^{6+}$ ions, and molecular diamagnetism which was estimated from Klemm constants.[27]

**EPR measurements**: Polycrystalline powder EPR spectra of **LiK-1** were recorded at frequencies ranging from 9.64 to 320 GHz at the high-field electron magnetic resonance facility at the National High Magnetic Field Laboratory in Tallahassee, FL, as described elsewhere.[28] Temperature variation was carried out from room temperature to 5 K. An Oxford Instruments Teslatron superconducting magnet sweepable between 0 and 17 T was used to apply the Zeeman field. In all experiments the modulation amplitudes and microwave power were adjusted for optimal signal intensity and resolution.

## Acknowledgements

U.K. acknowledges support from Jacobs University, the German Science Foundation (DFG-KO-2288/3-2) and the Fonds der Chemischen Industrie. A.M. thanks the German Science Foundation as well as the Fonds der Chemischen Industrie for continuous support over the years, furthermore the German-Israeli Foundation for Scientific Research & Development (GIF), and the European Union (MRTN-CT-2003-504880). This work was also supported by the CNRS and the University Paris-Sud 11 (UMR 8000). The help of Dr. Pedro de Oliveira in setting up experiments with NO is thankfully acknowledged. N.S. and J.v.T. would like to acknowledge the State of Florida and the NSF Core Operative Agreement grants DMR-0084173 and DMR-0520481 for financial support. Figures 1–3 were generated by Diamond Version 3.1e (copyright Crystal Impact GbR).

[1] a) This refers in a general sense to scenarios where "materials" grow with preferred orientations on surfaces influenced/directed by the surfaces' geometry: V. E. Henrich, P. A. Cox, *The Surface Science of Metal Oxides*, Cambridge University Press, Cambridge **1994**, p. 384; b) The process is quite common in the geosphere. This leads to situations where spaces with larger scale sizes (bulk condition comparable), but also up to smaller scales, are filled with minerals or water; the well-known geodes are objects of that type (see textbooks of mineralogy). The confinement induced changes in the water structure and dynamics, which are commonly substrate specific, play a key-role in the geosphere regarding the reactivity of mineral surfaces (see J. Wang, A. G. Kalinichev, R. J. Kirkpatrick, *J. Phys. Chem. B* **2005**, *109*, 14308–14313). Important information about that topic can be obtained from POM chemistry (see: A. Oleinikova, H. Weingärtner, M. Chaplin, E. Diemann, H. Bögge, A. Müller, *ChemPhysChem* **2007**, *8*, 646–649).

[2] Phospholipid vesicles are for instance the reaction vessels for many biomineralisation processes: in the spatially confined environments the biological systems can control the reaction conditions to achieve extraordinary morphologies (T. Douglas, in *Biomimetic Materials Chemistry* (Ed.: S. Mann), VCH, Weinheim, **1996**, p. 91).

[3] S. Mann, *Biomineralisation: Principles and Concepts in Bioinorganic Materials Chemistry*, Oxford University Press, Oxford, **2001**.

[4] a) W. Kaim, B. Schwederski, *Bioinorganic Chemistry: Inorganic Elements in the Chemistry of Life*, Wiley, Chichester, **1994**; see also L.-O. Essen, S. Offermann, D. Oesterhelt, K. Zeth, in *Biomineralisation: Progress in Biology, Molecular Biology and Application* (Ed.: E. Baeuerlein), Wiley-VCH, Weinheim, **2004**, p. 119; in this context the authors refer to the toxicity of $Fe^{II}$ for aerobic organisms in the sense that it reduces $O_2$ to the reactive superoxide anion $O_2^-$ and reacts with the peroxide in the Fenton reaction to form the highly reactive $OH^{\cdot}$ radical; b) J. Schemberg, K. Schneider, U. Demmer, E. Warkentin, A. Müller, U. Ermler, *Angew. Chem.* **2007**, *119*, 2460–2465; *Angew. Chem. Int. Ed.* **2007**, *46*, 2408–2413; c) A. Müller, S. Q. N. Shah, H. Bögge, M. Schmidtmann, *Nature* **1999**, *397*, 48–50.

[5] R. Contant, A. Tézé, *Inorg. Chem.* **1985**, *24*, 4610–4614.

[6] M. Zimmermann, N. Belai, R. J. Butcher, M. T. Pope, E. V. Chubarova, M. H. Dickman, U. Kortz, *Inorg. Chem.* **2007**, *46*, 1737–1740.

[7] a) S. S. Mal, U. Kortz, *Angew. Chem.* **2005**, *117*, 3843–3846; *Angew. Chem. Int. Ed.* **2005**, *44*, 3777–3780; b) D. Jabbour, B. Keita, L. Nadjo, U. Kortz, S. S. Mal, *Electrochem. Commun.* **2005**, *7*, 841–847; c) M. S. Alam, V. Dremov, P. Müller, A. V. Postnikov, S. S. Mal, F. Hussain, U. Kortz, *Inorg. Chem.* **2006**, *45*, 2866–2872; d) G. Liu, T. Liu, S. S. Mal, U. Kortz, *J. Am. Chem. Soc.* **2006**, *128*, 10103–10110; corrigendum: G. Liu, T. Liu, S. S. Mal, U. Kortz, *J. Am. Chem. Soc.* **2007**, *129*, 2408.

[8] C. Pichon, P. Mialane, A. Dolbecq, J. Marrot, E. Rivière, B. Keita, L. Nadjo, F. Sécheresse, *Inorg. Chem.* **2007**, *46*, 5292–5301.

[9] A. Müller, M. T. Pope, A. M. Todea, H. Bögge, J. van Slageren, M. Dressel, P. Gouzerh, R. Thouvenot, B. Tsukerblat, A. Bell, *Angew. Chem.* **2007**, *119*, 4561–4564; *Angew. Chem. Int. Ed.* **2007**, *46*, 4477–4480.

[10] S. S. Mal, N. H. Nsouli, M. H. Dickman, U. Kortz, *Dalton Trans.* **2007**, 2627–2630.

[11] Novel iron-substituted polyoxometalates and processes for their preparation: U. Kortz, S. S. Mal, USSN 11/728,142, patent filed on 23 March 2007.

[12] I. D. Brown, D. Altermatt, *Acta Crystallogr. Sect. A* **1985**, *41*, 244–247.

[13] B. Keita, Y. W. Lu, L. Nadjo, R. Contant, *Electrochem. Commun.* **2000**, *2*, 720–726.

[14] J. E. Toth, F. C. Anson, *J. Electroanal. Chem.* **1989**, *256*,361–370.

[15] B. Keita, A. Belhouari, L. Nadjo, R. Contant, *J. Electroanal. Chem.* **1998**, *442*, 49–57.

[16] B. Keita, L. Nadjo, *Electrochemistry of Polyoxometalates, Encyclopedia of Electrochemistry, Vol 7* (Eds.: A. J. Bard, M. Stratmann), Wiley-VCH, **2006**, pp. 607–700.

[17] B. Keita, F. Girard, L. Nadjo, R. Contant, R. Belghiche, M. Abbessi, *J. Electroanal. Chem.* **2001**, *508*, 70–80.

[18] B. Keita, A. Abdeljalil, L. Nadjo, R. Contant, R. Belghiche, *Langmuir* **2006**, *22*, 10416–10425.

[19] a) B. Keita, L. Nadjo, *J. Mol. Catal. A* **2007**, *262*, 190–215; b) L. Lisnard, P. Mialane, A. Dolbecq, J. Marrot, J. M. Clemente-Juan, E. Coronado, B. Keita, P. de Oliveira, L. Nadjo, F. Sécheresse, *Chem. Eur. J.* **2007**, *13*, 3525–3536; c) B. Keita, P. de Oliveira, U. Kortz, *Chem. Eur. J.* **2007**, *13*, 5480–5491.

[20] a) S. M. Gorun, S. J. Lippard, *Inorg. Chem.* **1991**, *30*, 1625–1630; b) R. Werner, S. Ostrovsky, K. Griesar, W. Haase, *Inorg. Chim. Acta* **2001**, *326*, 78–88; c) C. Cañada-Vilalta, T. A. O'Brien, E. K. Brechin, M. Pink, E. R. Davidson, G. Christou, *Inorg. Chem.* **2004**, *43*, 5505–5521.

[21] a) J. K. McCusker, C. A. Christmas, P. M. Hagen, R. K. Chadha, D. F. Harvey, D. N. Hendrickson, *J. Am. Chem. Soc.* **1991**, *113*, 6114–6124; b) C. Delfs, D. Gatteschi, L. Pardi, R. Sessoli, K. Wieghardt, D. Hanke, *Inorg. Chem.* **1993**, *32*, 3099–3103; c) A. Ozarowski, B. R. McGarvey, J. E. Drake, *Inorg. Chem.* **1995**, *34*, 5558–5566.

  

[22] a) *Magnetochemistry* (Ed.: R. L. Carlin), Springer, Berlin, **1986**. b) *Molecular Magnetism* (Ed.: O. Kahn), VCH, Weinheim, **1993**.
[23] L.-H. Bi, U. Kortz, S. Nellutla, A. C. Stowe, J. van Tol, N. S. Dalal, B. Keita, L. Nadjo, *Inorg. Chem.* **2005**, *44*, 896–903.
[24] a) U. Kortz, S. Nellutla, A. C. Stowe, N. S. Dalal, J. van Tol, B. S. Bassil, *Inorg. Chem.* **2004**, *43*, 144–154; b) U. Kortz, S. Nellutla, A. C. Stowe, N. S. Dalal, U. Rauwald, W. Danquah, D. Ravot, *Inorg. Chem.* **2004**, *43*, 2308–2317; c) B. S. Bassil, S. Nellutla, U. Kortz, A. C. Stowe, J. van Tol, N. S. Dalal, B. Keita, L. Nadjo, *Inorg. Chem.* **2005**, *44*, 2659–2665; d) S. Nellutla, J. van Tol, N. S. Dalal, L.-H. Bi, U. Kortz, B. Keita, L. Nadjo, G. Khitrov, A. G. Marshall, *Inorg. Chem.* **2005**, *44*, 9795–9806.
[25] R. Contant, *Inorg. Synth.* **1990**, *27*, 110.
[26] B. Keita, L. Nadjo, *J. Electroanal. Chem. Interfacial Electrochem.* **1988**, *243*, 87–103.
[27] S. G. Vulfson, *Molecular Magnetochemistry*, Gordon and Breach Science: Amsterdam, **1998**, p. 241.
[28] a) B. Cage, A. K. Hassan, L. Pardi, J. Krzystek, L. C. Brunel, N. S. Dalal *J. Magn. Reson.* **1997**, *124*, 495–498; b) A. K. Hassan, L. A. Pardi, J. Krzystek, A. Sienkiewicz, P. Goy, M. Rohrer, L. C. Brunel, *J. Magn. Reson.* **2000**, *142*, 300–312.

Received: September 10, 2007
Published online: December 28, 2007

  